

A Context Integrated Relational Spatio-Temporal Model for Demand and Supply Forecasting

Hongjie Chen,¹ Ryan A. Rossi,² Kanak Mahadik,² Hoda Eldardiry¹

¹Department of Computer Science, Virginia Tech
Blacksburg, Virginia 24060

²Adobe Research

San Jose, California 95110

jeffchan@vt.edu, rrossi@adobe.com, mahadik@adobe.com, hdardiry@vt.edu

Abstract

Traditional methods for demand forecasting only focus on modeling the temporal dependency. However, forecasting on spatio-temporal data requires modeling of complex non-linear relational and spatial dependencies. In addition, dynamic contextual information can have a significant impact on the demand values, and therefore needs to be captured. For example, in a bike-sharing system, bike usage can be impacted by weather. Existing methods assume the contextual impact is fixed. However, we note that the contextual impact evolves over time. We propose a novel context integrated relational model, *Context Integrated Graph Neural Network* (CIGNN), which leverages the temporal, relational, spatial, and dynamic contextual dependencies for multi-step ahead demand forecasting. Our approach considers the demand network over various geographical locations and represents the network as a graph. We define a demand graph, where nodes represent demand time-series, and context graphs (one for each type of context), where nodes represent contextual time-series. Assuming that various contexts evolve and have a dynamic impact on the fluctuation of demand, our proposed CIGNN model employs a fusion mechanism that jointly learns from all available types of contextual information. To the best of our knowledge, this is the first approach that integrates dynamic contexts with graph neural networks for spatio-temporal demand forecasting, thereby increasing prediction accuracy. We present empirical results on two real-world datasets, demonstrating that CIGNN consistently outperforms state-of-the-art baselines, in both periodic and irregular time-series networks.

Introduction

Demand and supply forecasting with spatio-temporal data is widely studied in several areas including intelligent transportation systems (Laptev et al. 2017; Mu et al. 2014; Wang and Cheng 2001) and infrastructure construction planning (Csiszár et al. 2019; Deb et al. 2017). For example, forecasting cellular data (Wang et al. 2015) demand in various places is critical for determining the ideal base station locations. Demand and supply forecasting is typically formulated as a time-series prediction problem (Liu et al. 2011; Willis and Northcote-Green 1983; Ziat et al. 2017). In spatio-temporal data analysis, there are multiple time-series recorded in various locations. The dependence among them

introduces the challenge of modeling relational and spatial dependencies for accurate forecasting. Another challenge is to incorporate influence from factors that cause fluctuations in demand and supply. Existing methods (Geng et al. 2019; Yao et al. 2018) make a simplifying assumption that environmental contexts introduce a fixed impact. However, we relax this assumption and consider dynamic contexts that have a time-evolving impact on demand and supply values.

To address the aforementioned challenges, we propose a novel GNN model, Context Integrated Graph Neural Network (CIGNN), which learns and incorporates temporal, relational, spatial, and dynamic contextual dependencies for time-series forecasting. Our approach represents the demand/supply network as a graph, and represents each type of context as a separate graph. Our method jointly learns a model to predict demand/supply and contextual time-series simultaneously. We design a fusion mechanism to model the contextual dependencies. To the best of our knowledge, this is the first work that integrates and exploits dynamic contexts in a unified way for spatio-temporal time-series predictions. We validate our model on two forecasting problems using real-world data: forecasting demand in a mobile call network and forecasting supply in a bike-sharing system on the *CallMi* and *BikeBay* datasets, respectively. The main contributions are summarized as follows:

- **Modeling Temporal, Relational, Spatial, and Dynamic Contextual Dependencies:** CIGNN performs demand forecasting by considering temporal, relational, spatial, and *dynamic* contextual dependencies. Existing methods do not capture the dynamic context. Table 1 qualitatively compares the abilities of various methods to model these dependencies.
- **Multi-source context Learning:** Contrary to existing work that uses only a single contextual type, CIGNN is capable to integrate multiple types of contextual features to improve forecasting.
- **Effectiveness:** CIGNN consistently outperforms previous methods with respect to both absolute error (MAE) and root mean square error (RMSE) for both *CallMi* and *BikeBay* datasets. CIGNN obtains average improvements of 5.7% (MAE) and 9.4% (RMSE) for *CallMi*; and 4.4% (MAE) and 2.3% (RMSE) for *BikeBay*.

	ARIMA	VAR	LSTM	STGCN	DCRNN	WaveNet	CIGNN
TEMPORAL	✓	✓	✓	✓	✓	✓	✓
SPATIAL				✓	✓	✓	✓
RELATIONAL				✓	✓	✓	✓
DYNAMIC CONTEXTUAL							✓

Table 1: Qualitative comparison of CIGNN to previous methods. Notably, CIGNN is the only approach that learns and incorporates temporal, relational, spatial, and contextual dependencies.

Related Work

Traditional time-series prediction methods such as Auto-Regressive Integrated Moving Average (ARIMA) and its variants (Hamilton 1994), suffer from several limitations. These methods (1) do not capture relational and spatial correlations, (2) cannot handle time-series with irregularities, and (3) generally perform poorly on long-term forecasting.

Forecasting based on deep learning allows the integration of complex temporal, relational, spatial, and contextual correlations to infer predictions. Previous work in spatio-temporal study leverages Convolutional Neural Networks (CNN) (Yao et al. 2018; Miao et al. 2019) and Graph Neural Networks (GNN) (Li et al. 2015; Scarselli et al. 2009; Wu et al. 2020; Bruna et al. 2013) to capture the spatial dependency. Recurrent Neural Networks (RNN) and their variants (Sutskever, Vinyals, and Le 2014; Wu et al. 2017) have also been used to capture temporal correlations.

Graph Neural Networks have shown unprecedented performance in different domains of study (Higuchi et al. 2019; Rossi 2018; Bruna et al. 2013; Kipf and Welling 2017). For instance, GraphSAGE (Hamilton, Ying, and Leskovec 2017) and FastGCN (Chen, Ma, and Xiao 2018), sample and aggregate neighborhood information to perform a graph classification task. Another line of study leverages GNN to perform forecasting (Zheng et al. 2020; Zhang et al. 2020; Song et al. 2020; Chen et al. 2019). Most of these works targets traffic forecasting improvements. For example, a diffusion convolution strategy has been proposed to predict the speed at one location by considering the speeds in proximity (Li et al. 2018). Another work utilized a GNN on both crime and traffic forecasting. (Wang et al. 2018) Other applications include city-wide bike demand forecasting (Defferrard, Bresson, and Vandergheynst 2016; Lin, He, and Peeta 2018) and weather prediction (Wilson, Tan, and Luo 2018). However, these methods ignore contextual information, thereby limiting their predictive performance.

Contextual features have a significant impact on demand and supply. For instance, ride-hailing demand is highly sensitive to precipitation. Existing approaches (Rong et al. 2018) assume a *static context*, which leads to a loss of information. By contrast, our approach integrates dynamic information to capture contextual impact. Moreover, existing work (Yao et al. 2018) incurs an increased cost of feature selection since their features are manually designed and integrated into the model. Our model, however, can handle various types of contextual information from multiple contextual sources simultaneously.

Context Integrated Graph Neural Network (CIGNN)

We propose a novel context integrated graph model, which leverages the temporal, relational, spatial, and contextual dependencies for demand and supply forecasting. Our method represents the demand network over locations as a graph. We define a demand graph, where nodes represent demand time-series, and context graphs (one graph for each type of context), where nodes represent contextual time-series.

We introduce our model *Context Integrated Graph Neural Network* (CIGNN) using a bike-sharing system as a running example. Given previous bike supply observations at various stations, CIGNN predicts the future supply by considering the following dependencies (also illustrated in Fig. 1):

Definition 1 (Temporal dependency) *Given a time-series $\mathbf{x} = [x_1 x_2 \dots x_T]$ where T is the length of the time-series. The temporal dependency is a mapping f from some observations prior to x_t (i.e. w = time-series lag) to x_t :*

$$[x_{t-1} x_{t-2} \dots x_{t-w}] \xrightarrow{f(\cdot)} x_t \quad (1)$$

The temporal dependency implies that future bike supply in a location relies on its historical supply.

The supply at a location also relies on those at others. We hereby define the relational and spatial dependency:

Definition 2 (Relational dependency) *Given a graph $G = (V, E)$, where V denotes the node set and E the edge set. Each node represents a bike station associated with a time-series that indicates the supply. Then, we define edges representing relational dependencies:*

$$E = \{(i, j) \mid \forall (i, j) \in |V| \times |V|, \text{s.t. } \mathbb{K}(\mathbf{x}_i, \mathbf{x}_j) \geq \lambda_r\} \quad (2)$$

where $\mathbf{x}_i, \mathbf{x}_j$ denote the time-series associated to nodes i and j , respectively. $|V|$ is the number of nodes and \mathbb{K} denotes a metric that measures the correlation between series.

Edges with a large weight $\mathbb{K}(\mathbf{x}_i, \mathbf{x}_j)$ imply dependency when the weight is greater than or equal to a threshold λ_r .

The key idea behind relational dependency is that similarly behaving time-series tend to be correlated in the future. For spatial dependency, we construct a graph differently.

Definition 3 (Spatial dependency) *Given a graph $G = (V, E, \mathbf{A})$ where V denotes the node set and E the edge set. Each node represents a location of a bike station. The adjacency matrix \mathbf{A} denotes the distance between nodes. We define the edges to represent spatial dependency:*

$$E = \{(i, j) \mid \forall (i, j) \in |V| \times |V|, \text{s.t. } \mathbf{A}_{ij} \geq \lambda_s\} \quad (3)$$

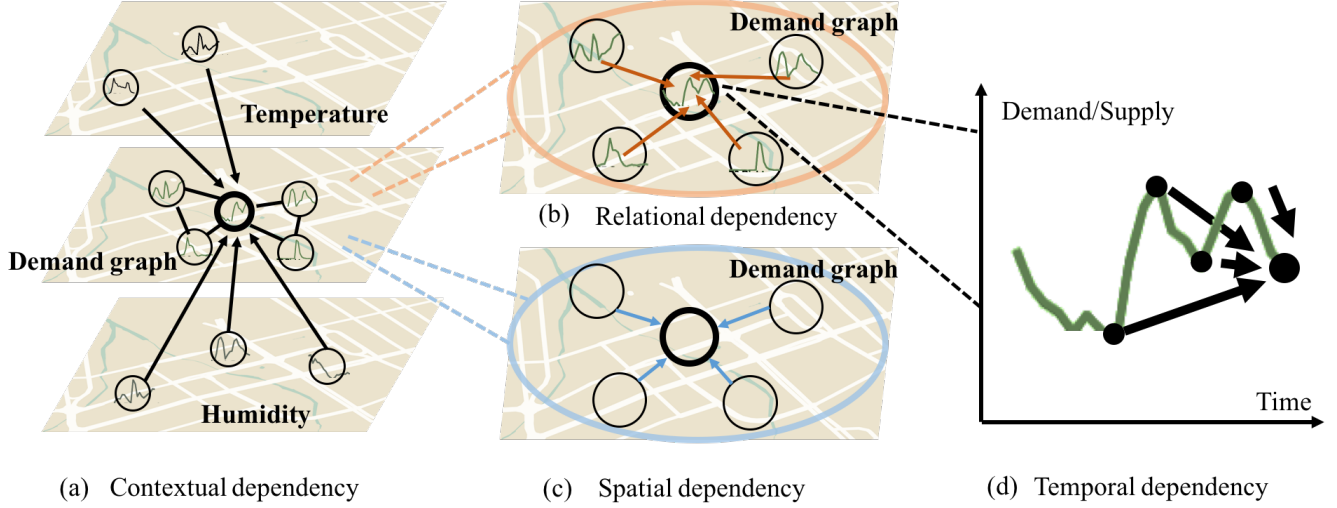


Figure 1: An illustration of spatial, temporal, relational, and contextual dependencies using only a node for simplicity. (a) Contextual dependency represents the impact of context (humidity and temperature) graphs on the demand graph. (b) Relational dependency represents the time-series correlation between nodes within a graph. (c) Spatial dependency represents the spatial correlation between nodes within a graph. (d) Temporal dependency represents the influence from history on future values.

Edges with a large weight \mathbf{A}_{ij} indicate potential dependency when the weight is greater than or equal to a threshold λ_s .

Definition 4 (Contextual dependency) Let a supply graph $G_s = (V_s, E_s)$ with a set of nodes V_s representing the bike stations that connected by edges in E_s . In addition, let a context graph $G_c = (V_c, E_c)$ with a set of nodes V_c representing the locations where contextual features are recorded (e.g., weather stations recording humidity), and connected by edges in E_c . Note that E_s and E_c are edges derived either from Definition 2 or Definition 3. We denote E_{sc} as edges connecting nodes in V_s with nodes in V_c .

$$E_{sc} = \{(i, j) \mid \forall (i, j) \in |V_s| \times |V_c|\} \quad (4)$$

To account for possibly more than one contextual type (e.g., if there are n contextual types), the definition can be extended to include all contextual types: $V_c = V_{c1} \cup \dots \cup V_{cn}$, $E_c = E_{c1} \cup \dots \cup E_{cn}$, for contextual types $c1, \dots, cn$.

In a bike-sharing system, the bike supply is impacted by weather such as temperature and precipitation, which are recorded in weather stations. We build a graph for temperature time-series and one for precipitation time-series.

Problem Formulation

Demand and supply forecasting in spatio-temporal data is a time-series prediction task where time-series are associated with locations. The task aims to learn a function f that predicts future values for each time-series. We refer to time-series in a graph as a *graph signal* (Furutani et al. 2019). A graph signal consists of signals from the same (graph) type. The demand/supply network and the $M - 1$ context networks are represented as a set of M graphs: $\mathcal{G} = \{G_1, G_2, \dots, G_M\}$. Each graph either represents the

Symbol	Description
$\mathcal{G}, M = \mathcal{G} $	a set of graphs and the number of graphs
T, T_w, T_h	length of time-series, window and horizon
G_i	the i^{th} graph, where $i \in \{1, \dots, M\}$
V_i, E_i, \mathbf{A}_i	nodes, edges and matrix in i^{th} graph
$N_i = V_i , P_i$	number of nodes and features in i^{th} graph
\mathcal{X}_i	the graph signal of the i^{th} graph
G, \mathcal{X}	a graph and its graph signal
\mathbf{A}, \mathbf{D}	Adjacency matrix and degree matrix
\mathbf{L}, \mathbf{I}	Laplacian matrix and the identity matrix
Θ_{*G}	the graph convolution layer
Φ	proposed fusion layer
$\theta, \mathbf{W}, \mathbf{b}, \mathbf{z}$	trainable parameters

Table 2: Summary of notation

demand/supply or a contextual type. For instance, to forecast the bike supply, the derived graphs include a bike supply graph, a temperature graph, and a humidity graph. The i^{th} graph is denoted as $G_i = (V_i, E_i, \mathbf{A}_i)$, where V_i and E_i represent the set of nodes and the set of edges in G_i , respectively. Nodes represent time-series with associated locations and edges represent the dependency between nodes. \mathbf{A}_i is the adjacency matrix that encodes geographical distance.

The graph G_i is associated with its corresponding graph signal $\mathcal{X}_i \in \mathbb{R}^{T \times N_i \times P_i}$, where T denotes the time span of interest, $N_i = |V_i|$ is the number of nodes, P_i is the number of node features. We use a subscript to denote which graph is referred, and a superscript to denote the time. For example, $\mathcal{X}_i^t \in \mathbb{R}^{N_i \times P_i}$ is the graph signal G_i at t .

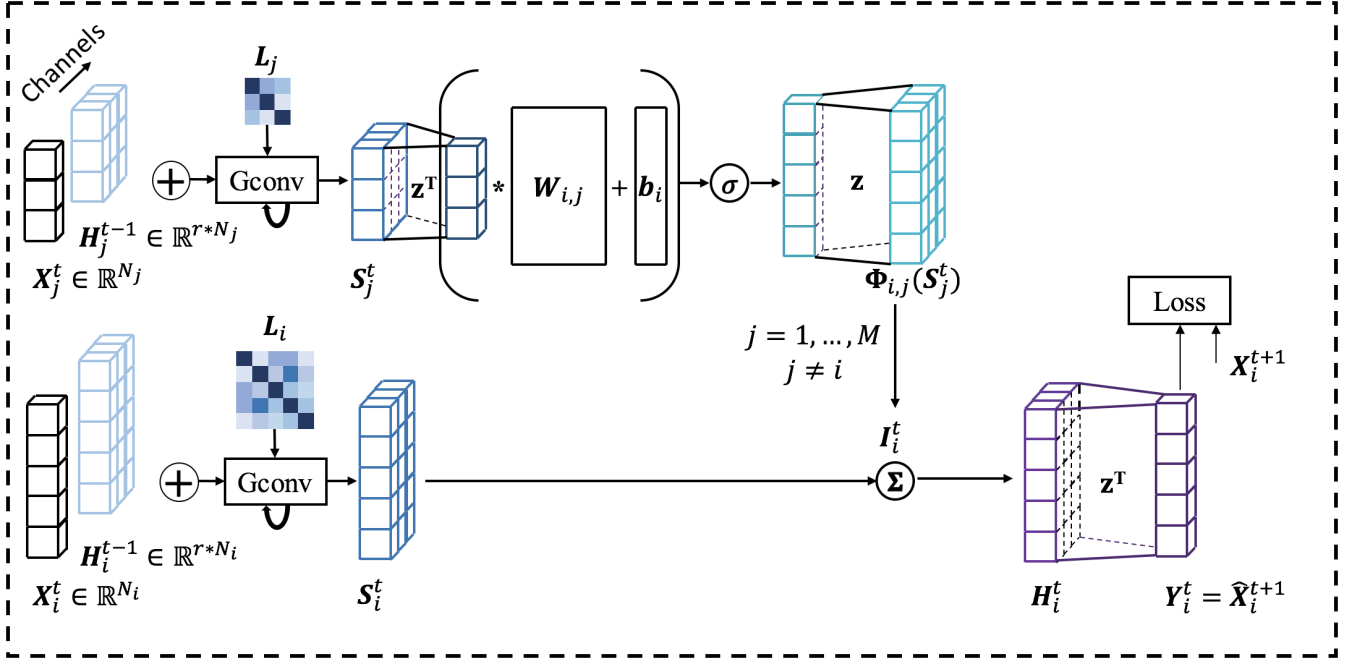


Figure 2: An overview of our CIGNN unit. Due to space limitations, only two graphs are displayed in the figure. In practice, CIGNN learns Φ for every combination of (i, j) where $i, j \in 1, 2, \dots, M, i \neq j$.

Given graphs and graph signals, a multi-step ahead time-series prediction task regarding T_w past observations and a horizon T_h is formulated as:

$$\left[\mathcal{X}_i^{t-T_w+1} \mathcal{X}_i^{t-T_w+2} \dots \mathcal{X}_i^t; G_i \right] \xrightarrow{f(\cdot)} \left[\mathcal{X}_i^{t+1} \mathcal{X}_i^{t+2} \dots \mathcal{X}_i^{t+T_h} \right] \\ i \in [1, \dots, M]$$

Graph Convolution to Exploit Relational and Spatial Features

Graph convolution is powerful to model the relational dependency and the spatial dependency (Wu et al. 2020). Given a graph G (constructed with either Definition 2 or Definition 3) and its graph signal \mathcal{X} , the graph convolution layer is defined as:

$$\begin{aligned} \Theta_{*G} \mathcal{X} &= \Theta(\mathbf{L}) \mathcal{X} \\ &= \Theta(\mathbf{Q} \mathbf{\Lambda} \mathbf{Q}^T) \mathcal{X} \\ &= \mathbf{Q} \Theta(\mathbf{\Lambda}) \mathbf{Q}^T \mathcal{X} \end{aligned} \quad (5)$$

where \mathbf{Q} is composed of eigenvectors of the graph Fourier transform. $\mathbf{\Lambda}$ is a diagonal matrix where each element is an eigenvalue of the normalized Laplacian matrix \mathbf{L} , defined with adjacency matrix \mathbf{A} and diagonal degree matrix \mathbf{D} :

$$\mathbf{L} = \mathbf{D}^{-\frac{1}{2}} (\mathbf{D} - \mathbf{A}) \mathbf{D}^{-\frac{1}{2}} \quad (6)$$

Strengthen Locality with Chebyshev Polynomials Approximation. Assuming that neighbor nodes have higher impacts, we reinforce the weights from the local neighbor-

hood. The graph kernel $\Theta(\mathbf{\Lambda})$ is extended to a series of polynomial bases as:

$$\Theta(\mathbf{\Lambda}) = \sum_{k=0}^{K-1} \theta_k \mathbf{\Lambda}^k \quad (7)$$

where K regulates the locality radius of nodes, and $\theta \in \mathbb{R}^k$ is a vector parameter of polynomial coefficients. A truncated Chebyshev polynomial expansion is adapted with Eq. 7 for computation efficiency:

$$\Theta_{*G} \mathcal{X} = \Theta(\mathbf{L}) \approx \sum_{k=0}^{K-1} \theta_k T_k(\tilde{\mathbf{L}}) \mathcal{X} \quad (8)$$

$$\tilde{\mathbf{L}} = \frac{2\mathbf{L}}{\lambda_{max}} - \mathbf{I} = \mathbf{L} - \mathbf{I}, \text{ assuming } \lambda_{max} = 2 \quad (9)$$

where $T_k(\tilde{\mathbf{L}})$ is the k^{th} Chebyshev polynomial at the scaled Laplacian $\tilde{\mathbf{L}}$ and \mathbf{I} is the identity matrix (Defferrard, Bresson, and Vandergheynst 2016; Tang, Li, and Yu 2019). λ_{max} is the greatest eigenvalue of \mathbf{L} , which is assumed as 2 to simplify the Eq. 9, as parameters can adapt to the change in scale during training (Kipf and Welling 2017). The Chebyshev polynomial reduces the time complexity from $\mathcal{O}(N^3)$ to $\mathcal{O}(K|\mathcal{E}|)$ where \mathcal{E} is the number of non-zero edges.

Graph convolution is separately applied on each graph:

$$\Theta_{*G_i}(\mathcal{X}_i) = \sum_{k=0}^{K-1} \theta_{k,i} \mathbf{L}_i^k \mathcal{X}_i, \quad i = 1, 2, \dots, M \quad (10)$$

Network Architecture

CIGNN is composed of units that take inputs at the current time step $\mathbf{X}_i^t \in \mathbb{R}^{N_i \times P_i}$ and hidden states from previous time step $\mathbf{H}_i^{t-1} \in \mathbb{R}^{r \times N_i \times P_i}$. With inputs and hidden states, CIGNN give hidden states of current step as $\mathbf{H}_i^t \in \mathbb{R}^{r \times N_i \times P_i}$, where r is the number of neurons. CIGNN is formulated as follows:

$$\mathbf{r}_i^t = \sigma(\mathbf{FC}_r(\Theta_{r*G_i}[\mathbf{X}_i^t \oplus \mathbf{H}_i^{t-1}])) \quad (11)$$

$$\mathbf{u}_i^t = \sigma(\mathbf{FC}_u(\Theta_{u*G_i}[\mathbf{X}_i^t \oplus \mathbf{H}_i^{t-1}])) \quad (12)$$

$$\mathbf{C}_i^t = \tanh(\mathbf{FC}_C(\Theta_{C*G_i}[\mathbf{X}_i^t \oplus (\mathbf{r}_i^t \odot \mathbf{H}_i^{t-1})])) \quad (13)$$

$$\mathbf{S}_i^t = \mathbf{u}_i^t \odot \mathbf{H}_i^{t-1} + (1 - \mathbf{u}_i^t) \odot \mathbf{C}_i^t \quad (14)$$

$$\mathbf{I}_i^t = \sum_{j=1, j \neq i}^M \Phi_{i,j}(\mathbf{S}_j^t) \quad (15)$$

$$\mathbf{H}_i^t = \mathbf{S}_i^t + \mathbf{I}_i^t \quad (16)$$

where Eq. 11-Eq. 14 are similar to the structure of Gated Recurrent Units (Chung et al. 2014). \mathbf{r} and \mathbf{u} denote the reset gate and update gate. \mathbf{FC} is a dense layer. Θ is the graph convolution layer, which captures either relational dependency or spatial dependency determined by what graph is used. The learned state \mathbf{S} incorporates both temporal, relational or spatial dependency. Φ is our proposed fusion layer that captures the contextual dependency across graphs, as defined in Definition 4. The subscript denotes different sets of parameters. The operator \oplus and \odot denotes concatenation operation and element-wise multiplication, respectively.

The fusion layer incorporate a graph with impacts from contextual graphs. \mathbf{I}_i in Eq. 15 captures impacts from other graphs on the i^{th} graph, as shown in Fig. 2. The structure of the fusion layer is designed in an interleaved manner:

$$\Phi_{(i,j)}(\mathbf{S}_j) = \sigma(\mathbf{z}[(\mathbf{W}_{i,j}^T \mathbf{z}^T \mathbf{S}_j^t + \mathbf{b}_j)]) \quad (17)$$

where σ denotes the sigmoid function and \mathbf{S}_j represents the hidden state from graph j . The weight parameters $\mathbf{W} \in \mathbb{R}^{N_j \times P_j \times P_i \times N_i}$, $\mathbf{b} \in \mathbb{R}^{N_i \times P_i}$ extracts relations between time-series across graphs, i.e., the contextual dependency. Note that \mathbf{W} has a similar form as E_{sc} defined in Eq. 4 when we consider the demand/supply graph and its contextual graphs. The parameter $\mathbf{z} \in \mathbb{R}^r$ is a mapping vector. Given the hidden state \mathbf{H}_i^t , the forecasting is conducted as:

$$\hat{\mathbf{X}}_i^{t+h} = \mathbf{z}_h^T \mathbf{H}_i^t, \quad h = 1, 2, \dots, T_h \quad (18)$$

where there is a \mathbf{z}_h for each horizon. Notice that the Eq. 18 models temporal dependency as in Definition 1. A goal function is then designed to minimize the prediction errors:

$$\underset{\theta_r, \theta_u, \theta_C, \mathbf{W}, \mathbf{b}, \mathbf{z}}{\operatorname{argmin}} \left| \hat{\mathbf{X}}_i^{t+h} - \mathbf{X}_i^{t+h} \right|, \quad (19)$$

$$i = 1, 2, \dots, M, \quad h = 1, 2, \dots, T_h$$

Experiments

In this section, we first introduce how the graphs are constructed, then we describe our experimental setup including two real-world datasets and previous approaches. Finally, we discuss our experimental results.

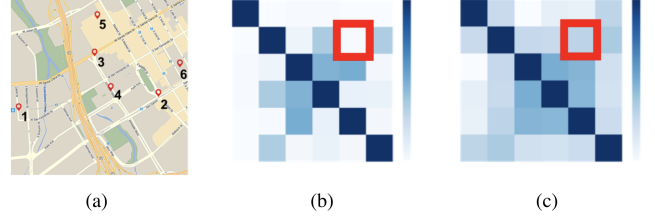


Figure 3: A comparison between Gaussian kernel matrix and Relational matrix. Dark color indicates higher correlations. (a). Some bike docks in San Jose. (b). The Gaussian kernel matrix. (c). The relational correlation matrix. The value between station 2 and 5 (marked by the red squares) is higher.

Graph Construction

We introduce two existing ways to construct a graph. One uses geographical distance to model spatial dependency. the other models the implicit correlations between time-series. Unless otherwise stated, we denote the adjacency matrix as $\mathbf{A} \in \mathbb{R}^{N \times N}$, and \mathbf{A}_{ij} is an element.

Distance-based Gaussian Kernel Matrix. Most existing work (Li et al. 2018; Yu, Yin, and Zhu 2018) derive an adjacency matrix with a truncated Gaussian kernel, such that $\mathbf{A}_{i,j}$ have higher values if node i and node j are nearer:

$$\mathbf{A}_{ij} = \begin{cases} \exp(-\frac{d(i,j)^2}{\sigma^2}), & \text{if } d(i,j) \leq \kappa \\ 0, & \text{otherwise} \end{cases} \quad (20)$$

where $d(i,j)$ denotes the geographical distance, σ denotes the standard deviation of distances and κ is a threshold.

Relational Matrix based on Correlation Coefficients. We observe in empirical studies that the Gaussian kernel matrix can fail to capture the hidden relational correlations between distant nodes. For example, in Fig. 3a, station 2 and station 5 are far from each other and the Gaussian Kernel matrix (Fig. 3b) suggests they have low correlations. However, they are highly correlated (Fig. 3c) in reality since people frequently commute between them along the straight road. Thus, we use the Detrended Cross-Correlation Analysis coefficient (DCCA coefficient) (Kristoufek 2014; Ide et al. 2017) to construct the *relational correlation matrix*.

The DCCA coefficient (Xu, Shang, and Kamae 2010) is a metric that infers correlations between series. It combines detrended cross-correlation analysis (DCCA) and detrended fluctuation analysis (DFA). Given two time-series $\mathbf{x}, \mathbf{y} \in \mathbb{R}^T$ and a window length l , the DCCA coefficient is defined as:

$$\rho_{DCCA}(\mathbf{x}, \mathbf{y}, l) = \frac{F_{DCCA}^2(\mathbf{x}, \mathbf{y}, l)}{F_{DFA}(\mathbf{x}, l) F_{DFA}(\mathbf{y}, l)} \quad (21)$$

where numerators and denominators are the average covariances and variances of the $T - s + 1$ windows (partial sums):

$$F_{DCCA}^2(\mathbf{x}, \mathbf{y}, l) = \frac{\sum_{s=1}^{T-l+1} f_{DCCA}^2(\mathbf{x}, \mathbf{y}, s)}{T-l} \quad (22)$$

$$F_{DFA}^2(\mathbf{x}, l) = \frac{\sum_{s=1}^{T-l+1} f_{DFA}^2(\mathbf{x}, s)}{T-l} \quad (23)$$

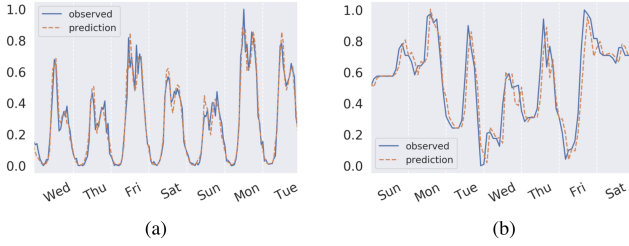


Figure 4: A comparison of time-series pattern. (a) The call demand during Dec. 25-31. (b) The bike supply in San Francisco during Aug. 25-31. Values are normalized for display. Note that *CallMi* shows more periodicity.

The partial sums are calculated with sliding windows across \mathbf{x} and \mathbf{y} . For each window with starting index s :

$$f_{DCCA}^2(\mathbf{x}, \mathbf{y}, s) = \frac{\sum_{t=s}^{s+l-1} (\mathbf{x}^t - \bar{\mathbf{x}}_s)(\mathbf{y}^t - \bar{\mathbf{y}}_s)}{l-1} \quad (24)$$

$$f_{DFA}^2(\mathbf{x}, s) = \frac{\sum_{t=s}^{s+l-1} (\mathbf{x}^t - \bar{\mathbf{x}}_s)^2}{l-1} \quad (25)$$

where $\bar{\mathbf{x}}_s$ is the average value of the window started with s .

The matrix is constructed with the pairwise correlations:

$$\mathbf{A}_{ij} = \begin{cases} \rho_{DCCA}(\mathbf{x}, \mathbf{y}, l), & \text{if } \rho_{DCCA}(\mathbf{x}, \mathbf{y}, l) \geq 0 \\ 0, & \text{otherwise} \end{cases} \quad (26)$$

Experimental Setup

To verify the effectiveness of CIGNN, we conduct experiments with two public real-world datasets. For both datasets, the following sets of hyperparameters are used: 0.01 (learning rate), 32 (number of neurons), 0.1 (learning rate decay ratio for every 10 epochs). We train for a maximum of 100 epochs using the Adam optimizer (Kingma and Ba 2014) and adapt an early stop strategy if the validation loss does not decrease for 10 consecutive epochs. All experiments are implemented using Python Tensorflow (v1.14) and run on Ubuntu 16.04 with 8 CPU cores and a memory of 32G.

- **Mobile Call Demand in Milan (*CallMi*)** (Barlacchi et al. 2015): *CallMi* contains call demand data in Milan from Nov. 2013 to Dec. 2013. The dataset contains temperature and humidity as contextual features. The city is partitioned into grids in the raw dataset, however, some grids have very few records. Therefore, we cluster grids into 162 mobile call nodes. There are 5 temperature nodes and 4 humidity nodes. Each of contextual nodes corresponds to a weather station. The time interval is an hour.
- **Bike-sharing Supply in the Bay Area (*BikeBay*)** (Ashqar, Elhenawy, and Rakha 2019): *BikeBay* contains the bike supply data in 70 dock stations in the Bay Area. The dataset was recorded from Aug. 2013 to Aug. 2015. It contains weather conditions as contextual data. There are 3 nodes for temperature, humidity, dew, sea level, and wind speed, respectively. The time interval is two hours.

Diversity of Datasets regarding Periodicity. The call demand time-series exhibit periodicity (Fig. 4a), while the bike supply time-series shows more irregularities (Fig. 4b). We chose datasets to demonstrate CIGNN’s capability to predict well on time-series with or without periodicity. The data are split chronologically into training, validation and testing sets in a ratio of 70%:10%:20%. When using the relational matrix, the window length l in Eq. 24 is set as 4. The graph convolution step in Eq. 10 is set as 1, for a previous study (Rossi et al. 2019) shows that a small step of graph convolution is more effective. Mean Absolute Error (MAE) is used as a loss measure to update parameters for all horizons in the training set. In evaluation, both MAE and Root Mean Square Error (RMSE) are calculated and compared:

$$MAE = \frac{1}{|\Omega|} \sum_{t \in \Omega} |\mathcal{X}_i^t - \hat{\mathcal{X}}_i^t|$$

$$RMSE = \sqrt{\frac{1}{|\Omega|} \sum_{t \in \Omega} (\mathcal{X}_i^t - \hat{\mathcal{X}}_i^t)^2}, \quad i = 1, 2, \dots, M$$

where Ω denotes the timestamps of measured samples.

Baseline Methods

We compare CIGNN to state-of-the-arts methods. However, we did not compare to (Yao et al. 2018) since it is only applicable on grid formatted data.

1. **HA** Historical Average. A prediction for a given time is the average of previous values at that same time (and day) over the past four weeks.
2. **ARIMA** Auto-Regressive Integrated Moving Average. The orders are (3, 0, 1), as in (Li et al. 2018).
3. **VAR** Vector Auto-Regressive is a multi-variate model that generalizes ARIMA to have multiple evolving variables.
4. **MM-LSTM** Multi-step multi-variate LSTM. The number of neurons is set as 64.
5. **DCRNN** (Li et al. 2018): Diffusion Convolution Recurrent Neural Network models spatial correlations with a diffusion process.
6. **STGCN** (Yu, Yin, and Zhu 2018): Spatio-Temporal Graph Convolutional Network models the spatial and temporal dependencies with a gating mechanism.
7. **Graph WaveNet** (Wu et al. 2019) Graph WaveNet leverages a self-adaptive adjacency matrix design to exploit spatial dependencies.

Results

Comparisons for multi-step ahead prediction Following common practice (Li et al. 2018; Yu, Yin, and Zhu 2018; Wu et al. 2019), we use six past observations to predict three steps ahead. Results are shown in Table 3. MAE and RMSE are evaluated for each horizon and on the average across horizons. Using dataset *BikeBay*, we further conduct more experiments with more data points (24) and a greater horizon (6) on the deep learning methods, as shown in Table 4. We observe the following:

<i>CallMi</i>									
Horizon	Metrics	HA	ARIMA	VAR	LSTM	STGCN	DCRNN	WaveNet	CIGNN
1	MAE	17.15	14.42	18.54	13.51	11.35	10.41	9.48	8.89
	RMSE	38.80	24.26	31.30	25.04	20.46	19.44	18.18	16.82
2	MAE	–	26.78	27.01	17.05	20.48	16.59	12.72	11.72
	RMSE	–	44.27	47.14	30.10	35.63	33.59	26.23	22.84
3	MAE	–	38.12	34.49	19.02	33.14	22.60	15.38	14.86
	RMSE	–	61.43	60.13	35.04	40.01	55.03	32.09	29.59

<i>BikeBay</i>									
Horizon	Metrics	HA	ARIMA	VAR	LSTM	STGCN	DCRNN	WaveNet	CIGNN
1	MAE	22.70	7.62	8.04	19.91	6.80	6.55	7.00	6.37
	RMSE	28.92	13.35	18.72	25.34	11.98	12.37	13.33	11.75
2	MAE	–	11.70	12.06	20.83	10.76	10.13	11.01	9.68
	RMSE	–	18.62	29.42	26.67	16.98	17.65	19.56	16.60
3	MAE	–	14.12	14.34	21.29	13.41	12.56	13.69	11.90
	RMSE	–	21.19	35.05	27.73	19.71	20.52	22.25	19.18

Table 3: A comparison using 6 observed data points to predict 3 steps ahead. MAE and RMSE of three horizons, their average, and average error reduction over VAR as a baseline for *CallMi* and *BikeBay*

- Deep learning based methods outperform traditional methods (HA, ARIMA and VAR) due to the latter methods’ limit of only modeling temporal dependency. Besides, HA can only predict one step ahead, and ARIMA fails to exploit the interactions across time-series.
- For deep learning methods, WaveNet outperforms DCRNN on *CallMi* but not on *BikeBay*, while CIGNN consistently outperforms STGCN, DCRNN and WaveNet. CIGNN also outperforms baselines when more observations and a larger horizon are considered.
- CIGNN outperforms previous best state-of-the-art mod-

<i>BikeBay</i>					
H	Metrics	STGCN	DCRNN	WaveNet	CIGNN
1	MAE	7.50	6.44	19.24	6.38
	RMSE	12.37	11.99	26.75	11.80
2	MAE	10.71	9.72	19.77	9.60
	RMSE	16.63	16.72	27.38	16.47
3	MAE	13.11	11.91	20.32	11.75
	RMSE	19.33	19.33	28.02	19.01
4	MAE	16.62	13.67	20.68	13.47
	RMSE	22.77	21.22	28.36	20.85
5	MAE	16.44	15.06	20.94	14.83
	RMSE	23.29	22.64	28.57	22.24
6	MAE	17.56	16.12	21.12	15.90
	RMSE	24.83	23.67	28.68	23.31

Table 4: A comparison of deep learning methods using 24 observed data points to predict 6 steps ahead on *BikeBay*.

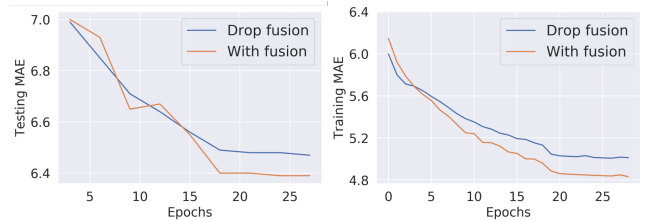


Figure 5: CIGNN with fusion outperforms the model without fusion, in both training and testing.

els on each dataset (improves over WaveNet on *CallMi* by 5.7% MAE and 9.4% RMSE and over DCRNN on *BikeBay* by 4.4% MAE and 2.3% RMSE).

Effectiveness of Fusion. To assess the effectiveness of our proposed fusion mechanism, we compared our approach to a variant that removes the fusion layer. We ran experiments on the *BikeBay* dataset and compared the two model for both training and testing loss, as shown in Fig. 5. Although CIGNN is initialized with a higher loss, its loss decreases faster. This shows that the fusion mechanism is effective in utilizing contextual factors on forecasting. We analyze the effectiveness of the Gaussian Kernel matrix and Relational matrix, added in appendix due to the limit of space.

Conclusion

To model non-linear temporal, relational, spatial, and contextual dependency in time-series predictions, we propose a novel Graph Neural Network approach for spatio-temporal data with dynamic contextual information. Our model employs a novel fusion mechanism to capture the dynamic contextual impact on demand.

Appendix

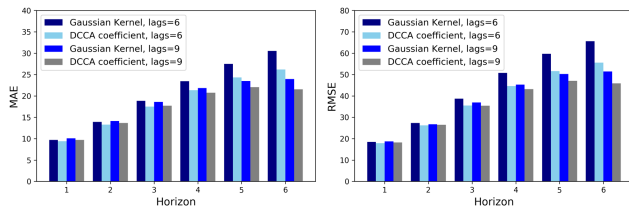


Figure 6: The MAE and RMSE comparison of models with adjacency matrix constructed by Gaussian Kernel and DCCA coefficient. DCCA coefficient-based model delivers better performance in both situations when lag number is 6 or 9.

Adjacency Matrix Analysis. To analyze and compare the effectiveness of the Gaussian Kernel matrix and the DCCA relational coefficients matrix, we ran experiments on the CallMi dataset using temporal lags 6 and 9. Fig. 6 shows the MAE and RMSE for a horizon of 6. The results show that: (1) Predictions based on the DCCA coefficient adjacency matrix are consistently more accurate than predictions based on the Gaussian kernel matrix. (2) The lag number has an impact on predicting values for a long horizon. Using 9 lags results in significantly better prediction results than using 6 lags. This demonstrates that CIGNN is better at learning long-term temporal dependencies.

References

- Ashqar, H. I.; Elhenawy, M.; and Rakha, H. A. 2019. Modeling bike counts in a bike-sharing system considering the effect of weather conditions. *Case Studies on Transport Policy* ISSN 2213-624X.
- Barlacchi, G.; De Nadai, M.; Larcher, R.; Casella, A.; Chitic, C.; Torrisi, G.; Antonelli, F.; Vespignani, A.; Pentland, A.; and Lepri, B. 2015. A multi-source dataset of urban life in the city of Milan and the Province of Trentino. *Scientific Data*.
- Bruna, J.; Zaremba, W.; Szlam, A.; and LeCun, Y. 2013. Spectral networks and locally connected networks on graphs. *arXiv preprint arXiv:1312.6203*.
- Chen, J.; Ma, T.; and Xiao, C. 2018. Fastgcn: fast learning with graph convolutional networks via importance sampling. *arXiv preprint arXiv:1801.10247*.
- Chen, W.; Chen, L.; Xie, Y.; Cao, W.; Gao, Y.; and Feng, X. 2019. Multi-range attentive bicomponent graph convolutional network for traffic forecasting. *arXiv preprint arXiv:1911.12093*.
- Chung, J.; Gulcehre, C.; Cho, K.; and Bengio, Y. 2014. Empirical evaluation of gated recurrent neural networks on sequence modeling. *arXiv:1412.3555*.
- Csiszár, C.; Csonka, B.; Földes, D.; Wirth, E.; and Lovas, T. 2019. Urban public charging station locating method for electric vehicles based on land use approach. *Journal of Transport Geography* 74: 173–180.
- Deb, C.; Zhang, F.; Yang, J.; Lee, S. E.; and Shah, K. W. 2017. A review on time series forecasting techniques for building energy consumption. *Renewable and Sustainable Energy Reviews* 74: 902–924.
- Defferrard, M.; Bresson, X.; and Vandergheynst, P. 2016. Convolutional neural networks on graphs with fast localized spectral filtering. In *Advances in neural information processing systems*, 3844–3852.
- Furutani, S.; Shibahara, T.; Akiyama, M.; Hato, K.; and Aida, M. 2019. Graph signal processing for directed graphs based on the hermitian laplacian. In *ECML-PKDD*.
- Geng, X.; Li, Y.; Wang, L.; Zhang, L.; Yang, Q.; Ye, J.; and Liu, Y. 2019. Spatiotemporal Multi-Graph Convolution Network for Ride-Hailing Demand Forecasting. *AAAI* doi:10.1609/aaai.v33i01.33013656.
- Hamilton, J. D. 1994. *Time series analysis*, volume 2. Princeton university press Princeton, NJ.
- Hamilton, W.; Ying, Z.; and Leskovec, J. 2017. Inductive representation learning on large graphs. In *Advances in neural information processing systems*, 1024–1034.
- Higuchi, M.; Matsutani, K.; Kumano, M.; and Kimura, M. 2019. Discovering Spatio-Temporal Latent Influence in Geographical Attention Dynamics. In *ECML-PKDD*. ISBN 978-3-030-10928-8.
- Ide, J.; Cappabianco, F.; Faria, F.; and Chiang-shan, R. L. 2017. Detrended partial cross correlation for brain connectivity analysis. In *NeurIPS*, 889–897.
- Kingma, D. P.; and Ba, J. 2014. Adam: A method for stochastic optimization. *arXiv preprint arXiv:1412.6980*.
- Kipf, T. N.; and Welling, M. 2017. Semi-Supervised Classification with Graph Convolutional Networks. In *ICLR*.
- Kristoufek, L. 2014. Measuring correlations between non-stationary series with DCCA coefficient. *Physica A: Statistical Mechanics and its Applications* 402: 291–298.
- Laptev, N.; Yosinski, J.; Li, L. E.; and Smyl, S. 2017. Time-series extreme event forecasting with neural networks at uber. In *ICLR*, volume 34, 1–5.
- Li, Y.; Tarlow, D.; Brockschmidt, M.; and Zemel, R. 2015. Gated graph sequence neural networks. *arXiv preprint arXiv:1511.05493*.
- Li, Y.; Yu, R.; Shahabi, C.; and Liu, Y. 2018. Diffusion Convolutional Recurrent Neural Network: Data-Driven Traffic Forecasting. In *ICLR*.
- Lin, L.; He, Z.; and Peeta, S. 2018. Predicting station-level hourly demand in a large-scale bike-sharing network: A graph convolutional neural network approach. *Transportation Research Part C: Emerging Technologies*.
- Liu, W.; Zheng, Y.; Chawla, S.; Yuan, J.; and Xing, X. 2011. Discovering Spatio-Temporal Causal Interactions in Traffic Data Streams. In *KDD*. ISBN 9781450308137. doi:10.1145/2020408.2020571.
- Miao, Y.; Han, J.; Gao, Y.; and Zhang, B. 2019. ST-CNN: Spatial-Temporal Convolutional Neural Network for crowd counting in videos. *Pattern Recognition Letters*.

- Mu, Y.; Wu, J.; Jenkins, N.; Jia, H.; and Wang, C. 2014. A spatial-temporal model for grid impact analysis of plug-in electric vehicles. *Applied Energy* .
- Rong, Y.; Xu, Z.; Yan, R.; and Ma, X. 2018. Du-Parking: Spatio-Temporal Big Data Tells You Realtime Parking Availability. In *SIGKDD*. ACM. ISBN 9781450355520.
- Rossi, R. A. 2018. Relational Time Series Forecasting. *KER* .
- Rossi, R. A.; Jin, D.; Kim, S.; Ahmed, N. K.; Koutra, D.; and Lee, J. B. 2019. From Community to Role-based Graph Embeddings. In *arXiv:1908.08572*.
- Scarselli, F.; Gori, M.; Tsoi, A. C.; Hagenbuchner, M.; and Monfardini, G. 2009. The Graph Neural Network Model. *IEEE Trans. Neural Netw.* ISSN 1941-0093. doi:10.1109/TNN.2008.2005605.
- Song, C.; Lin, Y.; Guo, S.; and Wan, H. 2020. Spatial-Temporal Synchronous Graph Convolutional Networks: A New Framework for Spatial-Temporal Network Data Forecasting. In *Proceedings of the AAAI Conference on Artificial Intelligence*, volume 34, 914–921.
- Sutskever, I.; Vinyals, O.; and Le, Q. V. 2014. Sequence to sequence learning with neural networks. In *NIPS*, 3104–3112.
- Tang, S.; Li, B.; and Yu, H. 2019. ChebNet: Efficient and Stable Constructions of Deep Neural Networks with Rectified Power Units using Chebyshev Approximations. *arXiv preprint arXiv:1911.05467* .
- Wang, B.; Luo, X.; Zhang, F.; Yuan, B.; Bertozzi, A. L.; and Brantingham, P. J. 2018. Graph-Based Deep Modeling and Real Time Forecasting of Sparse Spatio-Temporal Data. *ArXiv abs/1804.00684*.
- Wang, D.; and Cheng, T. 2001. A spatio-temporal data model for activity-based transport demand modelling. *IJGIS* 15(6): 561–585.
- Wang, S.; Zhang, X.; Zhang, J.; Feng, J.; Wang, W.; and Xin, K. 2015. An approach for spatial-temporal traffic modeling in mobile cellular networks. In *2015 27th International Teletraffic Congress*. IEEE.
- Willis, H. L.; and Northcote-Green, J. E. 1983. Spatial electric load forecasting: a tutorial review. *Proceedings of the IEEE* 71(2): 232–253.
- Wilson, T.; Tan, P.-N.; and Luo, L. 2018. A Low Rank Weighted Graph Convolutional Approach to Weather Prediction. In *ICDM*. IEEE.
- Wu, X.; Dong, Y.; Huang, C.; Xu, J.; Wang, D.; and Chawla, N. V. 2017. Uapd: Predicting urban anomalies from spatial-temporal data. In *ECML-PKDD*.
- Wu, Z.; Pan, S.; Chen, F.; Long, G.; Zhang, C.; and Philip, S. Y. 2020. A comprehensive survey on graph neural networks. *IEEE Transactions on Neural Networks and Learning Systems* .
- Wu, Z.; Pan, S.; Long, G.; Jiang, J.; and Zhang, C. 2019. Graph WaveNet for Deep Spatial-Temporal Graph Modeling. In *IJCAI*.
- Xu, N.; Shang, P.; and Kamae, S. 2010. Modeling traffic flow correlation using DFA and DCCA. *Nonlinear Dynamics* 61(1-2): 207–216.
- Yao, H.; Wu, F.; Ke, J.; Tang, X.; Jia, Y.; Lu, S.; Gong, P.; Ye, J.; and Zhenhui, L. 2018. Deep Multi-View Spatial-Temporal Network for Taxi Demand Prediction. In *AAAI*.
- Yu, B.; Yin, H.; and Zhu, Z. 2018. Spatio-Temporal Graph Convolutional Networks: A Deep Learning Framework for Traffic Forecasting. In *IJCAI*. doi:10.24963/ijcai.2018/505.
- Zhang, Q.; Chang, J.; Meng, G.; Xiang, S.; and Pan, C. 2020. Spatio-Temporal Graph Structure Learning for Traffic Forecasting. In *Proceedings of the AAAI Conference on Artificial Intelligence*, volume 34, 1177–1185.
- Zheng, C.; Fan, X.; Wang, C.; and Qi, J. 2020. Gman: A graph multi-attention network for traffic prediction. In *Proceedings of the AAAI Conference on Artificial Intelligence*, volume 34, 1234–1241.
- Ziat, A.; Delasalles, E.; Denoyer, L.; and Gallinari, P. 2017. Spatio-temporal neural networks for space-time series forecasting and relations discovery. In *ICDM*, 705–714. IEEE.